Shielded button electrodes for time-resolved measurements of electron cloud buildup

J.A. Crittenden[a,*], M.G. Billing[a], Y. Li[a], M.A. Palmer[a], J.P. Sikora[a]

[a]*CLASSE, Cornell University, Ithaca, NY 14853, United States*

Abstract

We report on the design, deployment and signal analysis for shielded button electrodes sensitive to electron cloud buildup at the Cornell Electron Storage Ring. These simple detectors, derived from a beam-position monitor electrode design, have provided detailed information on the physical processes underlying the local production and the lifetime of electron densities in the storage ring. Digitizing oscilloscopes are used to record electron fluxes incident on the vacuum chamber wall in 1024 time steps of 100 ps or more. The fine time steps provide a detailed characterization of the cloud, allowing the independent estimation of processes contributing on differing time scales and providing sensitivity to the characteristic kinetic energies of the electrons making up the cloud. By varying the spacing and population of electron and positron beam bunches, we map the time development of the various cloud production and re-absorption processes. The excellent reproducibility of the measurements also permits the measurement of long-term conditioning of vacuum chamber surfaces.

Keywords: storage ring, electron cloud

1. Introduction

The buildup of electron clouds (ECs) can cause instabilities and emittance growth in storage rings with positively charged beams. Low-energy electrons can be generated by ionization of residual gas, by beam particle loss and by synchrotron-radiation-induced photo-effect on the vacuum chamber walls. These electrons can generate secondary electrons, particularly when accelerated to high energy by the stored beam [1]. We report on studies performed in the context of the Cornell Electron Storage Ring Test Accelerator (CesrTA) program [2], an accelerator R&D program for future low-emittance electron and positron storage rings. The production of photoelectrons by synchrotron radiation is by far the dominant cause of electron cloud development at such high-energy storage rings [3]. Many techniques for measuring the EC density have been developed at CesrTA. One class of detectors samples the flux of cloud electrons on the wall of the beam-pipe. This paper describes the use of a shielded button electrode (SBE) as such an electron flux detector with sub-nanosecond time-resolving capability. The SBE is sometimes referred to as a shielded-pickup [4] or a shielded button pickup [5]. We outline several experimental techniques based on the performance of this type of detector to quantify cloud growth and decay mechanisms.

2. The Shielded Button Electrode Detector

Two 1.1-m-long sections located symmetrically in the east and west arc regions of the CESR ring were equipped with custom vacuum chambers as shown in Fig. 1. A retarding-field analyzer port is shown on the left end, and two SBE modules are shown near the right end of the chamber, each with two detectors. The SBEs incorporate beam-position monitor (BPM) electrode designs, but placed outside the beam-pipe behind a pattern of holes shielding them from the directly induced signal from the passing beam bunches. Two SBE electrodes are placed longitudinally, providing redundancy and two others are arranged transversely, providing laterally segmented sensitivity to the cloud electrons. The centers of the latter two electrodes are ±14 mm from the horizontal center of the chamber.

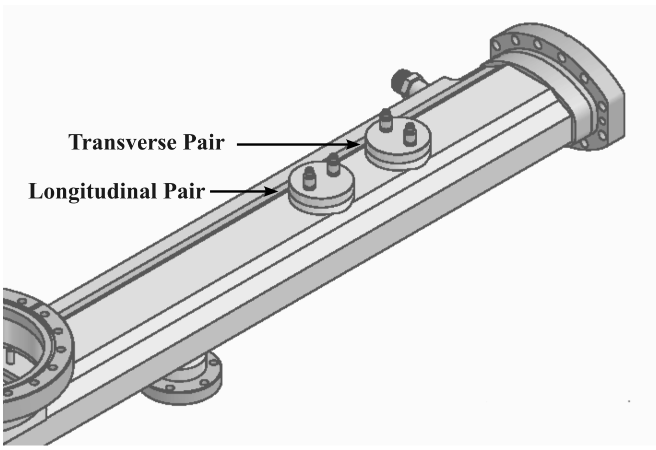

Figure 1: Custom vacuum chamber with shielded button electrodes. The SBEs, derived from beam-position monitor designs, are arranged in pairs: one pair along the beam axis, the other pair transverse.

Figure 2 shows schematically a cross-section of the SBE, the pattern of holes in the vacuum chamber allowing signal electrons to reach the button electrode, and the readout signal path.

*Corresponding author. Tel.: +1 6072554882
Email address: crittenden@cornell.edu (J.A. Crittenden)

[1]Work supported by the US National Science Foundation (PHY-0734867, PHY-1002467, and PHY-1068662), US Department of Energy (DE-FC02-08ER41538), and the Japan/US Cooperation Program

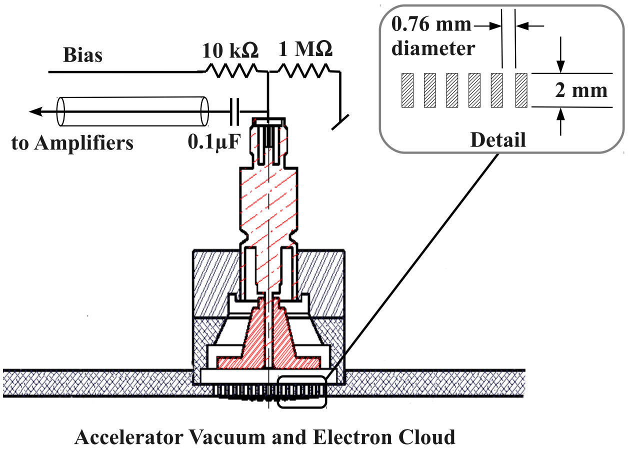

Figure 2: SBE detector design, biasing and readout. The 3:1 ratio of depth to diameter of the holes in the top of the beam-pipe effectively shields the collector electrode from the direct beam signal. A 50-V positive bias serves to prevent secondary electrons produced on the electrode from escaping.

The distance from the beam-pipe surface to the electrode is 3 mm. A DC bias relative to the grounded vacuum chamber is applied to the electrode through a 10 kΩ resistor. The signal is AC coupled to the 50 Ω coaxial cable through a 0.1 μF blocking capacitor which provides high pass filtering. A 1 MΩ bleeder resistor provides a local ground path to prevent the electrode from charging up when the bias circuit is disconnected. The front-end readout electronics comprise two Mini-Circuits ZFL-500 broadband amplifiers with 50 Ω input impedance for a total gain of 40 dB. Their bandwidth of 0.05-500 MHz is approximately matched to the digitizing oscilloscope used to record their output signals. Oscilloscope traces are recorded with 0.1 ns step size to 8-bit accuracy with auto-scaling, averaging over 8000 triggers. The fastest risetime recorded for EC signals has been less than 1 ns (see Sec. 3). In contrast to the measurements provided by commonly used retarding-field analyzers [6, 7], which integrate the incident charge flux to provide a steady-state signal current, our readout method provides time-resolved information on the cloud buildup, averaged over 8000 beam revolutions in order to reduce sensitivity to asynchronous high-frequency noise. The trigger rate is limited by the oscilloscope averaging algorithm to about 1 kHz. Since the beam revolution time is 2.5 μs, the cloud is sampled about once every 400 turns.

The hole pattern, shown in Fig. 3, consists of 169 holes of 0.76 mm diameter arranged in concentric circles up to a maximum diameter of 18 mm. The hole axes are vertical. The approximate 3:1 depth-to-diameter factor is chosen to shield effectively the detectors from the signal induced directly by the beam [8]. The transparency for vertical electron trajectories is 27%. Together with the 1×10^{-3} m^2 area of the hole pattern, the 50 Ω impedance and the 40 dB gain, this transparency results in a signal of 1.35 V for a perpendicular current density of 1 A m^{-2}.

A 50 V positive bias on the button electrode serves to eliminate contributions to the signal from escaping secondary electrons. Very few of these secondaries have kinetic energy sufficient to escape a 50 V bias. This choice of bias also provides sensitivity to cloud electrons which enter the holes in the vacuum chamber with low kinetic energy.

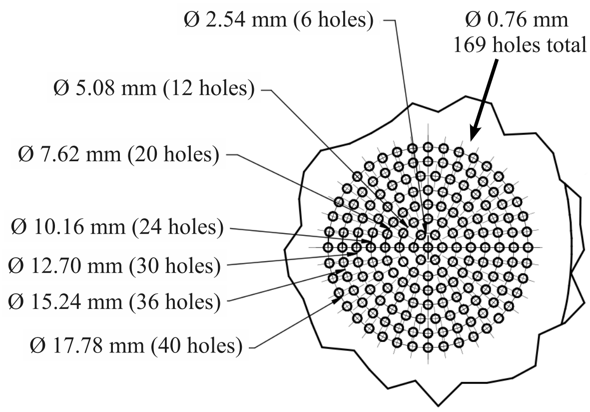

Figure 3: Hole pattern in the top of the vacuum chamber permitting signal electrons to reach the SBE. The 169 holes are centered on seven concentric circles of diameters ranging from 2.54 mm to 17.78 mm.

3. Measurement of Electron Cloud Buildup Dynamics

Figure 4 shows an example of a digitized SBE signal produced by two 5.3 GeV beam bunches each consisting of $4.8{\times}10^{10}$ positrons spaced 24 ns apart. The rms bunch length is 18 mm. Synchrotron radiation of critical energy 3.8 keV from the upstream dipole magnet is absorbed on the vacuum chamber wall (amorphous-carbon-coated aluminum) nearly simultaneously with the arrival of the positrons. The arrival time of the 60-ps-long bunch is indicated by the small directly induced signal which penetrated the shielding holes, shown at a time of 10 ns in Fig. 4. This small direct beam signal serves as a useful fiducial for determining the time interval between bunch passage and cloud electron arrival times at the button electrode.

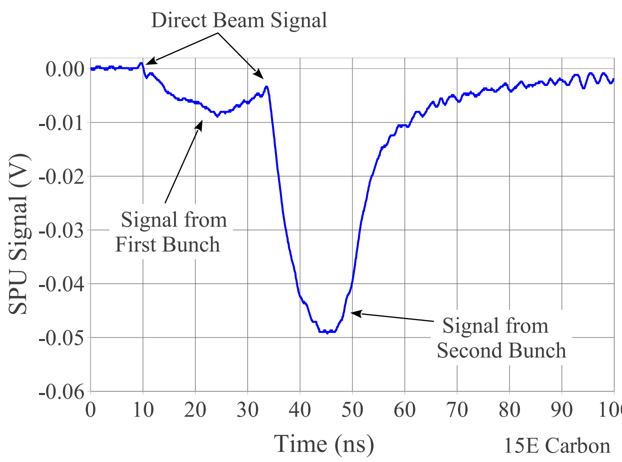

Figure 4: The SBE signal produced by two beam bunches spaced by 24 ns, each comprising $4.8{\times}10^{10}$ positrons.

The time characteristics of such signals carry much detailed information on EC development. The leading bunch seeds the cloud and produces photoelectrons which can eventually pass into the SBE detector. The signal from this first bunch is produced by the photoelectrons produced on the bottom of the vacuum chamber, since they are the first to arrive at the top of the chamber, accelerated by the positron bunch toward the detector above. The arrival times of the signal electrons are determined by the combination of production energy, beam acceleration, and the distance between the top and bottom of the vacuum chamber. The second signal peak induced by the trailing ("witness") bunch is larger, since it carries a contribution from the cloud present below the horizontal plane containing the beam when the bunch arrives. Since these cloud electrons have been produced by wall interactions during the preceding 24 ns, the size and shape of this second signal peak depend directly on the secondary yield characteristics of the vacuum chamber surface.

Figure 5 shows the signals obtained from two electron bunches of similar length and population as the positron bunches considered above. The primary source of synchrotron

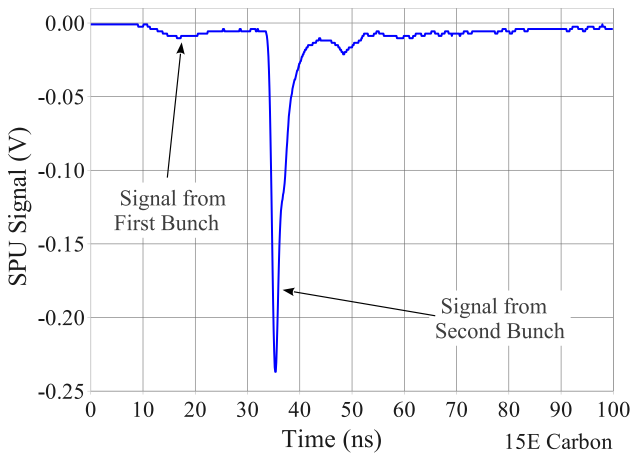

Figure 5: A pair of bunches consisting of $4.8{\times}10^{10}$ electrons spaced by 24 ns show a dramatic difference in the first and second bunch signals similar to that observed for the positron bunches. The second bunch signal has a much faster rising edge than the corresponding signal for a positron beam shown in Fig. 4.

radiation is of higher critical energy, 5.6 keV, since the source point is in a dipole magnet of 3 kG field, rather than 2 kG. In addition, the incident photon rate is about a factor of three higher, since the distance to the upstream dipole is 1 m rather than 3 m. The more dramatic difference between the signals from the first and second bunches results from the fact that the witness-bunch signal arises from cloud electrons located above the horizontal plane containing the beam at the bunch arrival time, giving a much steeper risetime and a peak signal about five times higher. This opposite beam kick also results in a signal of much shorter duration. The amplitude and time dependence of the leading bunch signal are sensitive to the production kinetic energy distribution of the photoelectrons, since they must overcome the beam kick in order to reach the detector. Time-sliced numerical simulations have shown that such electrons must be produced with hundreds of electron-volts of kinetic energy [4, 9]. These photoelectrons, like the photoelectrons producing the lead signal with a positron beam, must be produced by synchrotron radiation which has undergone sufficient reflection to be absorbed on the bottom of the beam pipe.

4. Measurement of Cloud Lifetime

Such time-resolving measurements of the cloud evolution provide sensitivity to its kinematic phase space distribution. The beam kicks, which can be controlled by varying the bunch population, accelerate cloud electrons to energies at and beyond the peak energy of the secondary emission curve [10]. Subsequent collisions with the vacuum chamber wall reduce the cloud kinetic energy. Eventually the secondary emission process is dominated by elastic reflection of the remaining low-energy electrons. The cloud lifetime is then determined by the material-specific elastic yield value of the surface.

Figure 6 illustrates a method of determining cloud lifetime, and therefore the elastic yield value, for an amorphous-carbon-coating. Overlaying the two-bunch signals obtained by varying

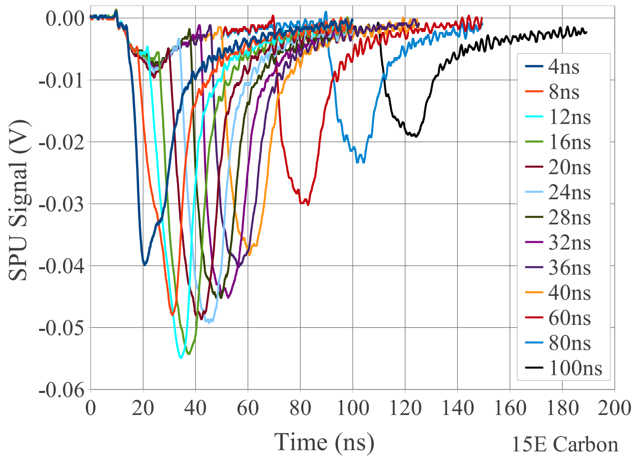

Figure 6: Overlay of thirteen two-bunch signals with delays varying from 4 to 100 ns, including the case of 24-ns delay shown in Fig. 4. The time dependence of EC buildup and decay are manifest. They result from the dependence of the various secondary emission processes on the energies of cloud electrons colliding with the vacuum chamber surface.

the delay in the arrival of the trailing bunch in 4-ns steps clearly shows both the buildup and decay of the cloud density. The various secondary emission processes contributing to buildup and decay [10] determine the delay which results in the maximum witness-bunch signal [11]. For the $4.8{\times}10^{10}$ bunch population shown here, the elastic yield property of the surface dominates the signal decay rate at delays greater than about 60 ns. For smaller values of the delay, the delay dependence of the witness-bunch amplitudes is governed by the relationship between bunch spacing, cloud kinematics and the size of the vacuum chamber. Numerical simulations have shown the elastic yield value for such a carbon coating to be less than 20%, similar to that found for a titanium-nitride coating [11]. In comparison, a similar study for an uncoated aluminum chamber found optimal agreement with the measured witness-bunch signals for an elastic yield value of 40%.

A similar witness-bunch study for an electron beam is shown in Fig. 7. While the signals from each witness bunch differ from those obtained with a positron beam as discussed in Sec. 3, the dependence on their delay times shows that detailed information on cloud buildup and decay, with the attendant information on vacuum chamber surface properties, can be obtained with an electron beam as well.

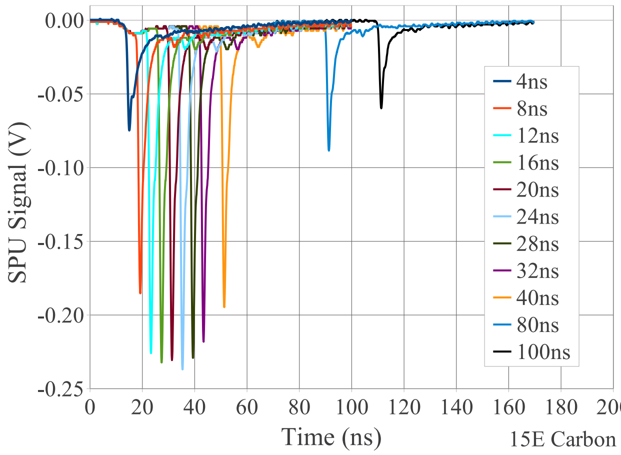

Figure 7: Overlay of eleven two-bunch signals with delays varying from 4 to 80 ns, including the case of 24-ns delay shown in Fig. 5.

5. Determination of Beam Conditioning Effects

The assessment of electron-cloud mitigation techniques necessarily includes their variation with beam dose. The secondary emission yields of copper and aluminum surfaces are known to decrease dramatically with beam dose, while such an effect is known to be smaller for TiN coatings [12]. The time-resolved measurements of the SBE in the custom vacuum chambers of CesrTA provide accurate determinations of beam conditioning effects owing to their reproducibility [13]. Figure 8 shows a comparison of two-bunch signals obtained in a TiN-coated aluminum chamber in April and June of 2011. During the intervening time period, CESR had operated as a high-current light source, so the beam dose was high. Using the calculation of synchrotron radiation power at this position in the ring, we convert from amp-hours to linear photon density to obtain an increase in dose from $1.4{\times}10^{25}\gamma$/m to $1.95{\times}10^{25}\gamma$/m over this intervening period. The TiN-coating shows no change in its secondary yield over this time and the measured two-bunch signals are reproducible at the level of a percent.

In contrast, the cloud-producing properties of an amorphous carbon coated chamber showed a strong dependence on radiation dose between May and December of 2010, as shown in Fig. 9. The SBE signals were reduced by about a factor of two for two 5.3 GeV bunches carrying $4.2{\times}10^{10}$ positrons each, 28 ns apart. The integrated linear photon density increased from $8.05{\times}10^{23}\gamma$/m to $1.82{\times}10^{25}\gamma$/m over this period, since the chamber had not been previously subjected to high-current running. The time dependence of the signals provides additional

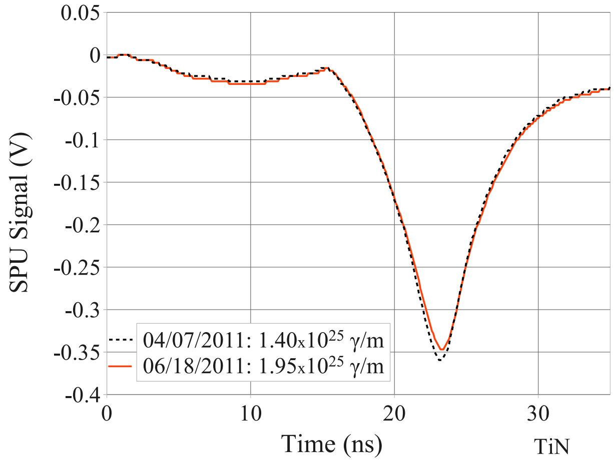

Figure 8: Comparison of SBE signals in April and June of 2011 obtained from a pair of 5.3 GeV positron bunches of population $8.2{\times}10^{10}$ separated by 14 ns. The change in the EC production properties of this TiN coating was negligible as the synchrotron radiation dose increased from $1.4{\times}10^{25}\gamma$/m to $1.95{\times}10^{25}\gamma$/m.

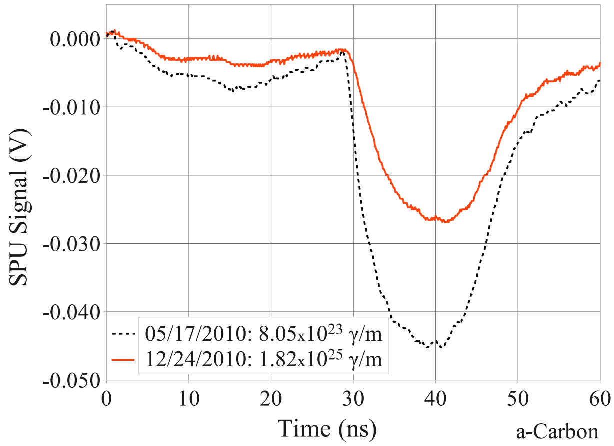

Figure 9: Comparison of two-bunch signals in May and December of 2010 in an amorphous-carbon-coated aluminum vacuum chamber shows a substantial reduction in cloud buildup. SBE signals from positron bunches of population $4.2{\times}10^{10}$ spaced by 28 ns were used for this purpose of comparison. The synchrotron radiation photon dose increased from $8.05{\times}10^{23}\gamma$/m to $1.82{\times}10^{25}\gamma$/m over these seven months.

information on the nature of the conditioning effect. The signal from the second bunch is much more sensitive to the secondary emission properties of the surface. Since the signal of the leading bunch was reduced in similar proportion, seeding a much less dense cloud, we can deduce that the secondary yield properties did not change appreciably. Indeed, full numerical simulations were consistent with a factor of two change in the photoelectron production rate and with no change in secondary yield [11, 13].

6. Summary

Time-resolved measurements of electron fluxes incident on the vacuum chamber wall in electron and positron storage rings have been shown to be provide sensitivity to each of the various physical processes contributing to electron cloud buildup and decay. We have employed a simple technique of placing an in-vacuum BPM-style button electrode behind a pattern of holes in the beam-pipe and digitizing the current signals obtained during and following the passage of a train of beam bunches. The method provides information on the scattering of synchrotron radiation within the pipe, the photoelectron production kinetic energy distribution, and the individual contributions of the various physical process contributing to secondary electron emission. Accurate determinations of cloud lifetime have been obtained, as have quantitative characterizations of photoelectron production and secondary emission properties of aluminum, amorphous carbon, diamond-like carbon and titanium-nitride coatings. The excellent reproducibility of the measurements on a time scale of months has permitted the determination of the beam-dose dependence of the surface properties of these electron cloud buildup mitigation techniques.

7. Acknowledgments

We wish to acknowledge contributions from the technical and administrative staffs of the Cornell Laboratory for Accelerator-based ScienceS and Education. This work is supported by the National Science Foundation under contract numbers PHY-0734867 and PHY-1002467 and by the US Department of Energy under contract numbers DE-FC02-08ER41538 and DE-SC0006505.

References

[1] M. A. Furman, Electron cloud effects in accelerators, in: R. Cimino, G. Rumolo, F. Zimmermann (Eds.), Proceedings of ECLOUD 2012: Joint INFN-CERN-EuCARD-AccNet Workshop on Electron-Cloud Effects, La Biodola, Elba, Italy, CERN-2013-002, CERN, Geneva, 2013, pp. 1–8. URL: http://cds.cern.ch/record/1606733.

[2] The CESR Test Accelerator Electron Cloud Research Program: Phase I Report, Technical Report CLNS-12-2084, LEPP, Cornell University, Ithaca, NY, 2013. URL: http://www.lepp.cornell.edu/public/CLNS/2012/CLNS12-2084/.

[3] K. Ohmi, Beam-photoelectron interactions in positron storage rings, Phys. Rev. Lett. 75 (1995) 1526–1529.

[4] J. A. Crittenden, Y. Li, X. Liu, M. A. Palmer, J. P. Sikora, S. Calatroni, G. Rumolo, N. Omcikus, Electron cloud modeling results for time-resolved shielded pickup measurements at CesrTA, in: K. Smolenski (Ed.), Proceedings of ECLOUD 2010: 49th ICFA Advanced Beam Dynamics Workshop on Electron Cloud Physics, Ithaca, NY, 2013, pp. 123–129. URL: http://accelconf.web.cern.ch/AccelConf/ECLOUD2010/papers/PST09.pdf.

[5] E. Mahner, T. Kroyer, F. Caspers, Electron cloud detection and characterization in the cern proton synchrotron, Phys. Rev. ST Accel. Beams 11 (2008) 094401.

[6] R. A. Rosenberg, K. C. Harkay, A rudimentary electron energy analyzer for accelerator diagnostics, Nucl. Instrum. Methods Phys. Res. A453 (2000) 507–513.

[7] J. R. Calvey, W. Hartung, Y. Li, J. A. Livezey, J. Makita, M. A. Palmer, D. L. Rubin, Comparison of electron cloud mitigating coatings using retarding field analyzers, 2014. URL: http://arxiv.org/abs/1402.1904, submitted to Nucl. Instrum. Methods Phys. Res. A.

[8] M. Sands, Energy Loss from Small Holes in the Vacuum Chamber, Technical Report PEP-253, SLAC, Stanford, CA, 1977.

[9] J. A. Crittenden, Y. Li, X. Liu, M. A. Palmer, J. P. Sikora, S. Calatroni, G. Rumolo, Electron cloud modeling results for time-resolved shielded pickup measurements at CesrTA, in: Proceedings of the 2011 Particle Accelerator Conference, New York, NY, 2011, pp. 1752–1754. URL: http://accelconf.web.cern.ch/AccelConf/PAC2011/papers/wep142.pdf

[10] M. A. Furman, M. T. F. Pivi, Probabilistic model for the simulation of secondary electron emission, Phys. Rev. ST Accel. Beams 5 (2002) 124404.

[11] J. A. Crittenden, J. P. Sikora, Electron cloud buildup characterization using shielded pickup measurements and custom modeling code at CesrTA, in: R. Cimino, G. Rumolo, F. Zimmermann (Eds.), Proceedings of ECLOUD 2012: Joint INFN-CERN-EuCARD-AccNet Workshop on Electron-Cloud Effects, La Biodola, Elba, Italy, CERN-2013-002, CERN, Geneva, 2013, pp. 241–250. URL: http://cds.cern.ch/record/1562274.

[12] J. Kim, D. Asner, J. Conway, S. Greenwald, Y. Li, V. Medjidzade, T. Moore, M. Palmer, C. Strohman, In-situ secondary electron yield measurement system at CesrTA, in: Proceedings of the 2011 Particle Accelerator Conference, New York, NY, 2011, pp. 1253–1255. URL: http://accelconf.web.cern.ch/AccelConf/PAC2011/papers/tup230.pdf

[13] J. A. Crittenden, Y. Li, X. Liu, M. A. Palmer, J. P. Sikora, S. Calatroni, G. Rumolo, S. Kato, R. P. Badman, Recent developments in modeling time-resolved shielded-pickup measurements of electron cloud buildup at CesrTA, in: Proceedings of the 2011 International Particle Accelerator Conference, San Sebastián, Spain, 2011, pp. 2313–2315. URL: http://accelconf.web.cern.ch/AccelConf/IPAC2011/papers/wepc135.p